Accepted Article

J Musculoskelet Neuronal Interact 2023

Journal of Musculoskeletal and Neuronal Interactions JMNI

Original Article

A novel methodology to estimate bone mechanical properties using dual-energy imaging to improve pedicle screw fixation

Carolina Solorzano Barrera[1,2], Isabelle Villemure[1,2,3], Carl-Éric Aubin[1,2,3]

[1]Institute of Biomedical Engineering, Polytechnique Montréal, Montréal, Canada;
[2]Research Center, Sainte-Justine University Hospital Center, Montréal, Canada;
[3]Department of Mechanical Engineering, Polytechnique Montréal, Montréal, Canada;

Abstract

Objective: To develop a methodology to improve the representation of the mechanical properties of a vertebral finite element model (FEM) based on a new dual-energy (DE) imaging technology to improve pedicle screw fixation. **Methods**: Bone-calibrated radiographs were generated with dual-energy imaging technology in order to estimate the mechanical properties of the trabecular bone. Properties were included in regions of interest in four vertebral FEMs representing heterogeneity and homogeneity, as a realistic and reference model, respectively. Biomechanical parameters were measured during screw pull-out testing to evaluate pedicle screw fixation. **Results**: Simulations with property distributions deduced from dual-energy imaging characterization (heterogeneous models) induced an increase in biomechanical indicators versus with a homogeneous representation, implying different behaviors for the subject-specific models. **Conclusion**: The presented methodology allows a patient-specific representation of bone quality in a FEM using new DE imaging technology. Consideration of individualized bone distribution in a spinal FEM improves the perspective of orthopedic surgical planning over otherwise underestimated results using a homogeneous representation.

Keywords: Dual-Energy Radiography, Finite Element Modeling, Pedicle Screw, Subject-Specific Modeling

Introduction

Vertebral bone is composed of trabecular and cortical bone tissue, providing the vertebral body a structural resistance to different types of loads withheld throughout a lifetime. Trabecular bone has been shown to be distributed heterogeneously within the vertebral body, where some regions are denser than others like the pedicle area[1], to provide such resistance. The constant change of loads accords the bone an anisotropic behaviour, consequently altering its mechanical properties[2]. Therefore, the bone mineral density (BMD) varies considerably between certain regions in the vertebral body[3,4], between vertebral levels[5], and even between individuals according to their age[6,7], as the evolution of bone density degradation leads for example to osteoporosis. Several studies have reported mathematical relationships to relate BMD and mechanical properties of interest that act on the vertebrae, such as the Young's modulus[3,8-11]. These relationships give an insight into better understanding the macro- and micro-structural behaviour of trabecular bone. Such understanding is particularly valuable to improve methods of screw fixation in spine surgery.

During spine surgery, instrumentation is needed to correct a deformity or treat a fracture where contoured rods are connected to pedicle screws. Pedicle screws need a proper purchase to sustain the loads exerted to correct

Carl-Éric Aubin reports grants from the Natural Sciences and Engineering Research Council of Canada (Industrial Research Chair Program with Medtronic of Canada), and outside of the current work, contracts with Medtronic. Carolina Solorzano Barrera and Isabelle Villemure have nothing to declare.

Corresponding author: Carl-Éric Aubin, Ph.D., P.Eng., Full Professor, NSERC/ Medtronic Industrial Research Chair in Spine Biomechanics, Polytechnique Montréal, Department of Mechanical Engineering, P.O. Box 6079, Downtown Station, Montreal (Quebec), H3C 3A7 Canada
E-mail: carl-eric.aubin@polymtl.ca

Edited by: G. Lyritis
Accepted 16 July 2023

the deformity and maintain it during the time needed to fuse the spine. For a given screw diameter and length, the fixation strength depends on the quality of the trabecular bone[12,13] and the thickness of the cortical bone traversed by the screw trajectory. The risk of pedicle screw failure has been reported in 0.8 to 27% of the cases[14,15], with screw dimension and trajectory being important determinants[16]. Additionally, poor bone quality (as found with osteoporosis) contributes to screw plowing and poor anchoring, and thus screw fixation planning should be considered differently from healthy vertebrae[13,17].

To improve pedicle screw anchorage during surgery, experimental testing of standard pull-out tests has been performed on cadaveric or foam specimens[12,18,19], but these limit the very diverse representation of vertebral characteristics in the adult spine deformity population. As an alternative, finite element modeling (FEM) can provide detailed biomechanical analysis and numerically simulate pull-out tests to evaluate the performance of the screw/vertebra interaction[16,20-23]. These models can be designed with a generic geometry and average mechanical properties, which intended to provide a realistic representation of the instrumentation simulation[24-27].

The spine geometry for FEMs can be obtained via imaging modalities such as computer tomography (CT) by generating volumes of interest and modeling a mesh around the surfaces created[28]. Other modalities include quantitative computer tomography (qCT), where the grey values on the images are correlated with known phantom densities to estimate the volumetric bone density of human vertebrae[11,29], and micro-CT, where the properties of single bone human specimen can be analyzed at the sub-tissue level[9,30,31], thus estimating mechanical properties. However, most of reported spine FEMs include only isotropic mechanical properties, limiting a realistic representation of the bone density variation. Moreover, CT or qCT requires correlating density and stiffness values with measured gray levels, a relatively long, complex, and expensive process in clinical practice. Also, these imaging techniques impose high levels of ionizing radiation on the patient[32], which limits their clinical use.

We recently acquired an off-label version of a low-dose multi-energy imaging system with the capacity of acquiring simultaneously bi-planar (lateral and frontal) radiographs of a patient in a standing, physiological weight-bearing position. Two X-ray fan beam tubes are used along with respective photon-counting detectors to simultaneously acquire upright high-resolution images. This system uses a technology of dual-energy (DE) absorptiometry to modulate a low and high X-ray energy into the tissues. Following the Beer-Lambert's law, bone and soft tissue can be visually separated according to their absorptiometry coefficients, which are energy dependent. Additionally, this system generates calibrated bone-targeted images which provide high-resolution information of the geometry and the value of bone mineral density of the vertebrae and pelvis. Estimation of the mechanical properties of trabecular bone can therefore be possible and thus be implemented into an existing vertebral finite element model to further study pedicle screw anchorage. The methodology to acquire said properties is the main purpose of this study as the dual-energy imaging system is a new prototype and its capabilities have yet to be exploited.

The objective of this study was to develop a methodology to improve the representation of the mechanical properties of the vertebral bone based on a new dual-energy imaging technology. An existing 3D vertebral finite element model will be used to evaluate the feasibility of this methodology and compare biomechanical parameters on pedicle screw fixation to previous studies.

Materials and Methods

Dual-energy radiographic images

As described previously, the dual-energy (DE) imaging system generates biplanar images of a standing patient. However, in order to have full control over the production of these images, in this feasibility assessment study we worked with a company-provided image simulator that generates synthetic biplanar radiographs in postero-anterior (PA) and lateral (LAT) view in DICOM format. The synthetic images have the same properties as the ones obtained directly from the imaging system.

The process to obtain the synthetic images through the image simulator depends on a previously acquired CT-scan of the spine of the patient. A calibration is done to mismatch the voxel values corresponding to bone tissue to pixel values in a planar image grid. To generate a realistic synthetic image, the acquisition parameters in the image simulator can be set similar to the DE imaging system such as the voltage, current, collimation filter, and more (Figure 1).

The image simulator can generate four different types of synthetic radiographs depending on the calibration parameters initially set: a contour-enhanced image, a polymethyl methacrylate (PMMA) calibrated image, an aluminum (AL) calibrated image, and a hydroxyapatite (HA) density calibrated image which simulates the bone mineral density of the acquired bone structures. Hydroxyapatite is a mineral found in calcium apatite which has similar properties to human bone mineral. The PMMA and aluminum calibrated images simulate respectively soft and bone tissue due to their similar absorptiometry coefficient. For both PMMA and aluminum calibrated images, the DICOM scale attribute is "mm of PMMA" and "mm of AL" respectively. For the hydroxyapatite calibrated images, this scale is "g/cm^2" as the images are calibrated with the density of this mineral. The pixel intensity value for HA-calibrated radiographs is therefore shown in the unit of bone mineral density (g/cm^2).

For this study, the radiographic images of the spine were generated from a test case derived from an open access CT scan from the dataset acquired by the Department of Radiology at the University of Washington and published online by the Department of Computing at Imperial College London (BioMedIA)[33,34]. The simulation acquisition

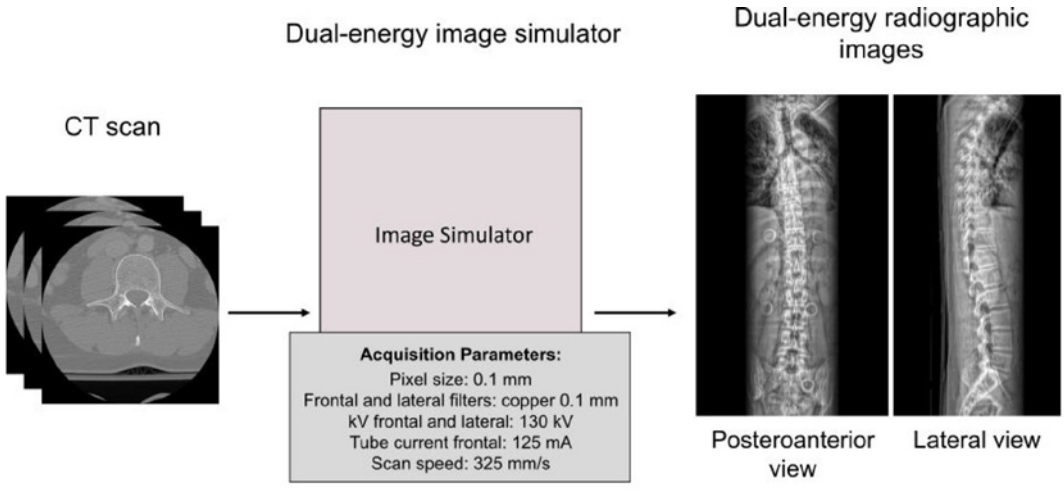

Figure 1. For the purpose of the feasibility study, the DE radiographic images were synthetically generated using available CT-scan from BioMedIA[33,34], using the simulated image acquisition parameters shown above. Four sets of the DE radiographic images were generated to simulate the density of the acquired spine structures: 1) contour-enhanced image, 2) polymethyl methacrylate (PMMA) calibrated image (soft tissue), 3) aluminum (AL) calibrated image (bone tissue), and 4) hydroxyapatite (HA) density calibrated image.

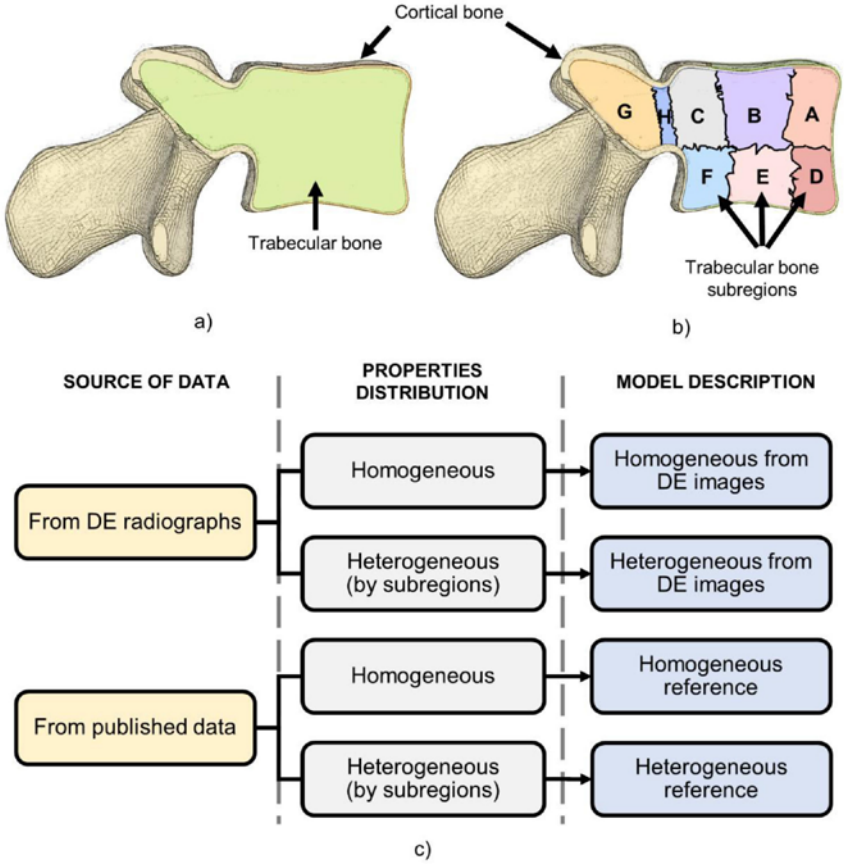

Figure 2. Isotropic FEMs of L3. a) A homogeneous model with both cortical and trabecular bone elements. b) A heterogeneous model with trabecular elements divided into 8 subregions and a cortical bone layer. The trabecular bone subregions are named A through H as follows: A) trabecular superior-anterior, B) trabecular superior-central, C) trabecular superior-posterior, D) trabecular inferior-anterior, E) trabecular inferior-central, F) trabecular inferior-posterior, G) trabecular posterior elements, and H) trabecular pedicle region. c) Diagram of the four vertebral models of this study.

Table 1. Estimated parameters from bi-planar dual-energy radiographs for the homogeneous model for: a) the trabecular bone, and b) the cortical bone. The estimated volumetric bone mineral density is shown in bold.

Parameters	Lateral view	Posteroanterior view	Both views
a) Trabecular bone			
Area (cm^2)	12.636	15.907	-
Average pixel intensity (g/cm^2)	1.040	1.329	-
Bone mineral content (g)	13.141	21.141	17.141
Depth (cm)	4.372	3.716	-
Volume (cm^3)	55.248	59.105	57.176
Volumetric bone mineral density (g/cm^3)	0.238	0.358	**0.298**
b) Cortical bone			
Area (cm^2)	5.902	4.729	-
Average pixel intensity (g/cm^2)	1.157	1.474	-
Bone mineral content (g)	6.828	6.971	6.899
Depth (cortical thickness) (cm)	0.289	0.738	-
Volume (cm^3)	1.706	3.490	2.598
Volumetric bone mineral density (g/cm^3)	4.003	1.997	**3.000**

Table 2. Computed parameters from bi-planar dual-energy radiographs for the heterogeneous vertebral model. The estimated volumetric bone mineral density is shown in bold as average vBMD (average from the lateral and posteroanterior view).

Parameters	Lateral view								Posteroanterior view				
Subregions of trabecular bone	A	B	C	D	E	F	G	H	Superior	Inferior	Right pedicle	Left pedicle	Both pedicles
Area (cm^2)	2.23	1.93	2.01	2.40	2.01	2.07	-	0.95	8.46	7.37	0.66	0.68	-
Average pixel intensity (g/cm^2)	0.66	0.92	1.17	0.54	1.20	1.49	-	1.04	1.29	1.35	0.93	1.21	-
Bone mineral content (g)	1.46	1.77	2.36	1.29	2.41	3.08	-	0.98	10.89	9.96	0.62	0.48	0.69
Depth (cm)	4.37	4.37	4.37	4.37	4.37	4.37	-	-	1.24	1.24	-	-	-
Volume (cm^3)	9.73	8.45	8.78	10.50	8.80	9.03	-	0.77	10.48	9.12	0.76	0.78	0.77
Volumetric bone mineral density (g/cm^3)	0.15	0.21	0.27	0.12	0.27	0.34	-	1.28	0.37	0.29	0.82	0.61	0.90
Average volumetric bone mineral density (g/cm^3)	**0.26**	**0.29**	**0.32**	**0.20**	**0.28**	**0.31**	**0.32**	**0.90**					

parameters were 130 kV and 125 mA for X-ray tube voltage and current, respectively, with a 0.1 mm copper filter. Pixel size of the images was set at 0.1 mm.

Definition of the vertebral models

From the simulated DE radiographs, the HA-calibrated images were used in this study to estimate the mechanical properties of the test case (referred thereafter as mechanical properties from DE images) to build an analytic subject-specific FEM. Moreover, a reference FEM was built, for comparison purposes, using published mechanical properties (referred thereafter as reference mechanical properties). For this feasibility study, the methodology was tested for the 3rd lumbar vertebra (L3), as the same vertebral FEM was used and validated in previous studies[16,35].

Four isotropic FEMs of L3 were created with two different trabecular bone distributions derived from the DE radiographs or from published trabecular bone mineral density, thereafter estimating the mechanical properties using published mathematical equations[36]: 1) averaged (homogeneous) model and 2) derived from the subject-specific images and averaged over small regions of interest

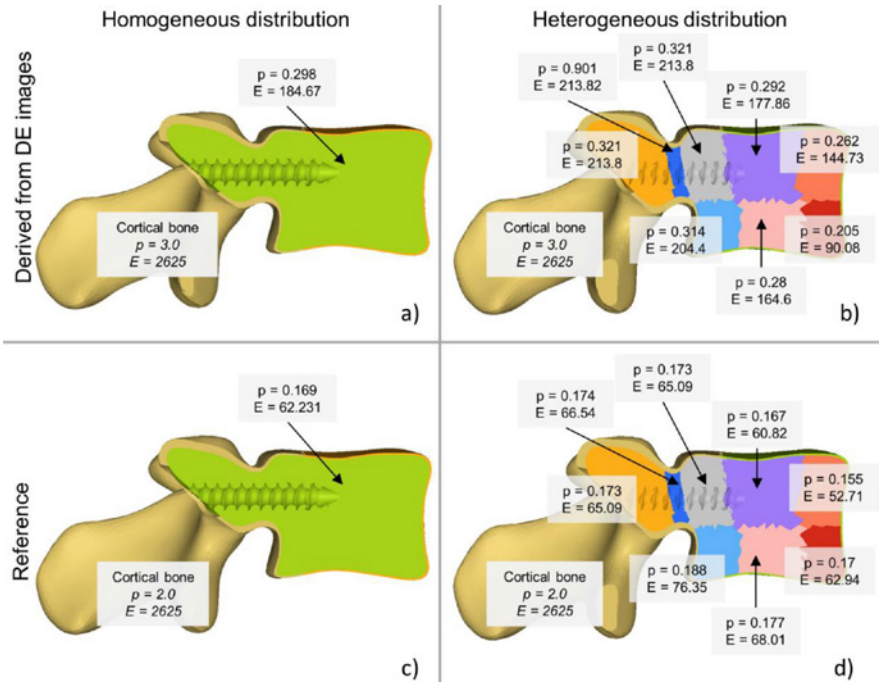

Figure 3. Mechanical properties of the four L3 vertebral models: a) homogeneous model from DE images, b) heterogeneous model from DE images, c) homogeneous reference model, and d) heterogeneous reference model. Values of volumetric bone mineral density (ρ, in g/cm^3) and Young's modulus (E, in MPa) are shown over each region for trabecular and cortical bone.

(heterogeneous) model, as shown in Figure 2.

For the heterogeneous models, eight different subregions (A-H) were defined to differentiate the mechanical properties of the anterior and posterior parts of the vertebral body as well as the superior and inferior regions (Figure 2b), following the work of Zhao et al. (2009)[37] and Wagnac et al. (2012)[38]. The posterior elements were also separated from the vertebral body, with two subregions in the pedicles. These subregions consider critical areas where BMD changes depending on the load transmission throughout the spine, such as the pedicle area and the anterior region of the vertebral body, which have high- and low-density values respectively[3,4].

Estimation of volumetric bone mineral density

Estimation of volumetric bone mineral density from dual-energy HA-calibrated radiographs

The pixel intensity values of the HA-calibrated radiographs obtained from the image simulator were defined as surface bone mineral density (g/cm^2). The volumetric bone mineral density (vBMD) was computed in the trabecular region for the homogeneous model and the 8 regions of interest (ROI) for the heterogeneous model for each radiograph using ImageJ (ImageJ 1.53a, National Institutes of Health, USA, Maryland). The surface area and the average pixel intensity value within each ROI was computed using a measuring tool in ImageJ. Average pixel intensity was converted as HA mineral density (g/cm^2) using the corresponding DICOM attributes.

From the surface area and calculated density, the analytic approach from Carter et al. (1992)[39] was followed to estimate the volumetric bone mineral density (g/cm^3), adding a 3D perspective into the estimation. Bone mineral content (BMC) was computed as *BMC=A*BMD*, where A is the surface area and BMD is the bone mineral density (or average pixel intensity value) from the selected ROI. Next, the depth of the ROI was estimated to assess a 3D perspective of the ROI's shape. To simplify the process, the volumetric shape of the trabecular bone on the vertebral body ROI was assumed as a rectangular prism. From the LAT image, the length of the vertebral body was measured to estimate the PA view depth, and conversely for the PA image. For the pedicle region, the shape was assumed as a cylindrical prism. Afterwards, the volume was estimated as *Volume=depth*A*. Finally, the volumetric bone mineral density was estimated as $vBMD = \frac{BMC}{volume}$.

This process was followed on both PA and LAT radiographic images for the homogeneous (Table 1) and for the heterogeneous (Table 2) models. The posterior elements' parameters were estimated using the trabecular superior-posterior subregion since their densities are similar. The cortical bone vBMD was estimated by creating

Table 3. Mechanical properties computed from published data for the homogeneous and heterogeneous L3 vertebral reference model. Young's modulus was estimated using Equation 1. The remaining mechanical properties were obtained from previous published data.

Mechanical Properties	Homogeneous model		Heterogeneous model								References
	Trabecular bone	Cortical bone	Trabecular bone (subregions)								
			A	B	C	D	E	F	G	H	
Volumetric bone mineral density (g/cm^3)	0.169	2.0	0.16	0.17	0.17	0.17	0.18	0.19	0.17	0.18	Trabecular: [3,44]; Cortical: [16]
Young's modulus (MPa)	62.23	2625	52.7	60.8	65.0	62.9	68.0	76.4	65.2	66.5	Trabecular: [36] Cortical: [16]
Poisson ratio	0.25	0.3	0.2	0.2	0.2	0.2	0.2	0.2	0.25	0.25	Homogeneous: [16]; Heterogeneous: [38]
Yield stress (MPa)	1.95	105	1.65	1.87	1.97	1.91	2.05	2.25	1.97	1.97	Homogeneous: [16]; Heterogeneous: [56]
Hardening modulus (MPa)	16.3	875	8.5	7	8.5	8.1	12.5	12.5	7	7	Homogeneous: [16]; Heterogeneous: [38]
Hardening exponent	1	1	1	1	1	1	1	1	1	1	
Failure plastic strain	0.04	0.04	0.082	0.06	0.082	0.08	0.104	0.104	0.06	0.06	
Plasticity maximum stress (MPa)	2.6	140	2.65	2.3	2.65	2.6	3.25	3.25	2.3	2.3	

Table 4. Mechanical properties computed from dual-energy radiographs for the homogeneous and heterogeneous L3 model. Young's modulus was estimated using Equation 1. The remaining mechanical properties were set from published data[16,38,40,56].

Mechanical Properties	Homogeneous model		Heterogeneous model							
	Trabecular bone	Cortical bone	Trabecular bone (subregions)							
			A	B	C	D	E	F	G	H
Volumetric bone mineral density (g/cm^3)	0.298	3.0	0.26	0.29	0.32	0.20	0.28	0.31	0.32	0.90
Young's modulus (MPa)	184.67	2625	144.73	177.86	213.82	90.08	164.61	204.43	213.82	213.82
Poisson ratio	0.25	0.3	0.2	0.2	0.2	0.2	0.2	0.2	0.25	0.25
Yield stress (MPa)	1.92	105	1.65	1.87	1.97	1.91	2.05	2.25	1.97	1.97
Hardening modulus (MPa)	16.3	875	8.5	7	8.5	8.1	12.5	12.5	7	7
Hardening exponent	1	1	1	1	1	1	1	1	1	1
Failure plastic strain	0.04	0.04	0.082	0.06	0.082	0.08	0.104	0.104	0.06	0.06
Plasticity maximum stress (MPa)	2.6	140	2.65	2.3	2.65	2.6	3.25	3.25	2.3	2.3

a singular rectangular subregion around the outer edge of the vertebral body with a thickness of around 1 mm, and thus was considered homogeneous for all models.

Estimation of reference volumetric bone mineral density from published data

The volumetric bone density for the reference model (homogeneous and heterogeneous) was estimated from the reported work of Banse et al. (2001) (Table 3). Based on the reported 48 samples of 8 lumbar vertebrae, the average density values were applied to the entire trabecular bone of the vertebra. The average of all obtained volumetric bone mineral densities was used as the single value of volumetric bone mineral density for the homogeneous model. As for the heterogeneous model, an analogous approach of average by subregion was used.

Computation of the mechanical properties

The mechanical properties of cortical and trabecular bones were represented by a Johnson-Cook elastoplastic law[40]. The Young's modulus (MPa) was defined from the vBMD according to the equation published by Keller et al. (1994) (Equation 1). Other mechanical properties, such as the Poisson's ratio, the yield stress (MPa) the hardening modulus (MPa), the hardening exponent, the failure plastic strain, and the plasticity maximum stress (MPa), were obtained from

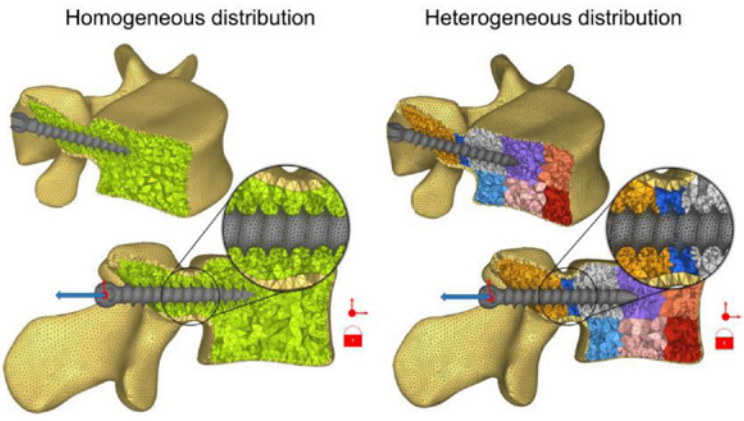

Figure 4. Meshed models with homogeneous and heterogeneous distribution with pedicle screw inserted in the right pedicle. Tetrahedral elements are seen in the trabecular bone surfaces. A closed-up view of the meshing between the screw model and the trabecular bone is displayed. A schematic representation of the boundary conditions with a fixation on the anterior nodes of the vertebral body and an in-line constraint of the screw is shown in red. Displacement rate direction on the screw is shown on with a blue arrow.

previous studies that used an inverse finite element method from experimental tests[38,40,41].

$$E=1.89\ vBMD^{1.92} \quad (1)$$

Equation 1 was used to estimate the Young's modulus for the homogeneous and heterogeneous models, from the trabecular vBMD of DE radiographs (Tables 1 and 2) and the trabecular vBMD was estimated from published data (Table 3). Cortical bone's mechanical properties were defined from the published literature. The mechanical properties computed from published data and derived from DE radiographs are shown in Tables 3 and 4, respectively, and in Figure 3.

Vertebral finite element model

The baseline FEM geometry of L3 used for all models in this study was first extracted from the SM2S (Spine Model for Safety and Surgery) model corresponding to a CT-scan of a healthy 32-year-old male volunteer in the 50th percentile with no back problems, which was previously developed within the framework of the iLab International Laboratory[24,41-43]. The model was then adapted with the properties of the tested case but maintained the baseline geometry of the model. It includes its vertebral body, the pedicles, and posterior elements. The cortical bone had a thickness varying between 1.0 to 1.5 mm, considering regional thickness[44,45]. Trabecular and cortical bone was meshed with 4 node tetrahedral elements whose characteristic size was 0.5 mm to 1 mm in the vicinity of the screws[16,46,47]. The mesh size and distribution on this model was tested for convergence in a previous study[16]. The FEM was generated using Hyperworks v2014 (Altair Engineering Inc., 2014, USA, Michigan).

The homogeneous L3 models had only the trabecular and cortical bone volumes. The heterogeneous L3 models were modified so the trabecular bone boundaries were separated into the 8 subregions defined in section "Definition of vertebral models". Figure 4 shows the resulting four vertebral FEMs.

Pedicle screw pull-out simulation

The pedicle screw used in this model was a 40-mm-long, 6.5-mm-diameter cylindrical screw with a single evenly spaced thread (CD Horizon Legacy screw). The screw was modeled as a rigid body with 0.5 mm shell triangular elements. The screw was inserted into the right pedicle of the L3 FEM in a straight-forward trajectory (Figure 4). A penalty-based contact was used at the bone-screw interface with a Coulomb-type friction coefficient of 0.2 and a minimal gap of 0.03 mm[16]. Fixed boundary conditions were applied in the external nodes of the anterior portion of the vertebral body[16]. The screw head was constrained with a slide link condition so it would slide out without an off-axis displacement during the simulation, which consisted of a displacement rate of 0.1 mm/ms to create axial load until the peak force was reached. The solver used for these quasi-static simulations was RADIOSS v2013 (Altair Engineering Inc., 2013, USA, Michigan).

From the pull-out simulations, three dependent parameters were post-processed to evaluate the performance of the pedicle screw fixation[16]: the peak pull-out force (MPa), the bone-screw interface initial stiffness (N/mm) and the distribution of maximum stress in the bone around the screw (MPa). The peak-pull-out force was reported as the maximum pull-out force recorded in the force-displacement curve. The initial stiffness was calculated for the most linear initial part of the slope of

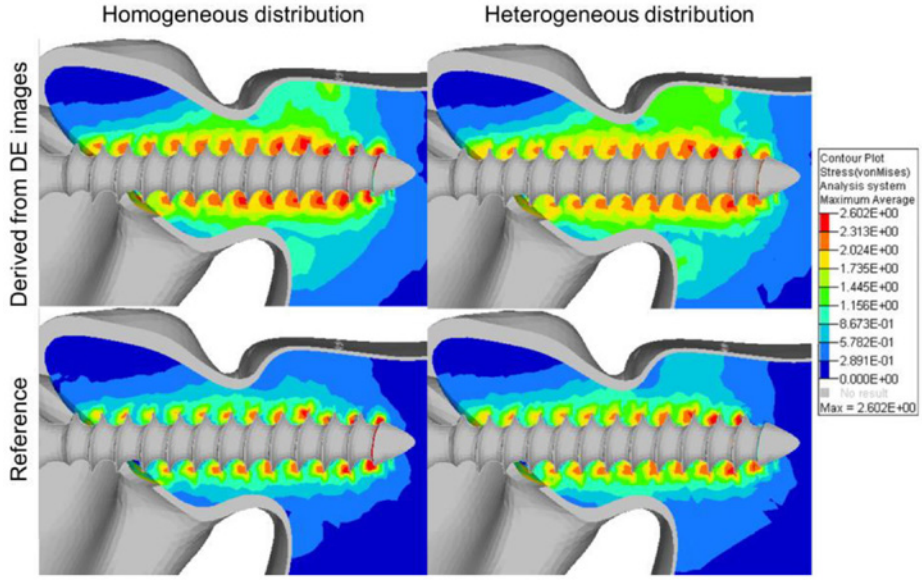

Figure 5. Von Misses stress distribution in the trabecular bone after the pedicle screw pull-out simulation for the four models. A color-coded legend shows the maximum stress presented on the model elements, red as the maximum value to blue as the lowest value. Images were captured for each model at their own peak pull-out force, which is manifested at a different time for each one.

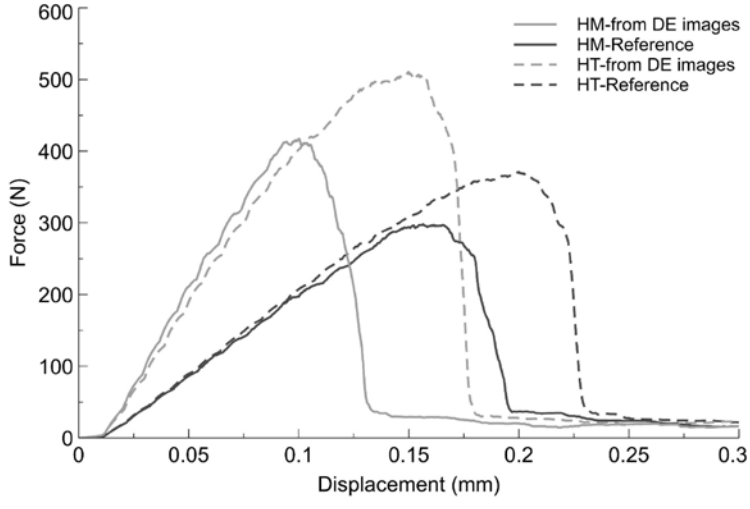

Figure 6. Force-displacement curves for all vertebral models. Models with properties derived from DE images (light grey) reach peak force at a smaller displacement, when compared to the reference (dark grey). Homogeneous models (HM) are shown in bold and heterogeneous models (HT) are shown with dashed lines.

force-displacement curve. Finally, the maximum stress distribution was calculated as the Von Misses stress distribution using the HyperView v2013 tool (Altair Engineering Inc., 2013, USA, Michigan).

Results

For the four models tested, the maximum stress in the trabecular bone were located at the screw threads, distributed

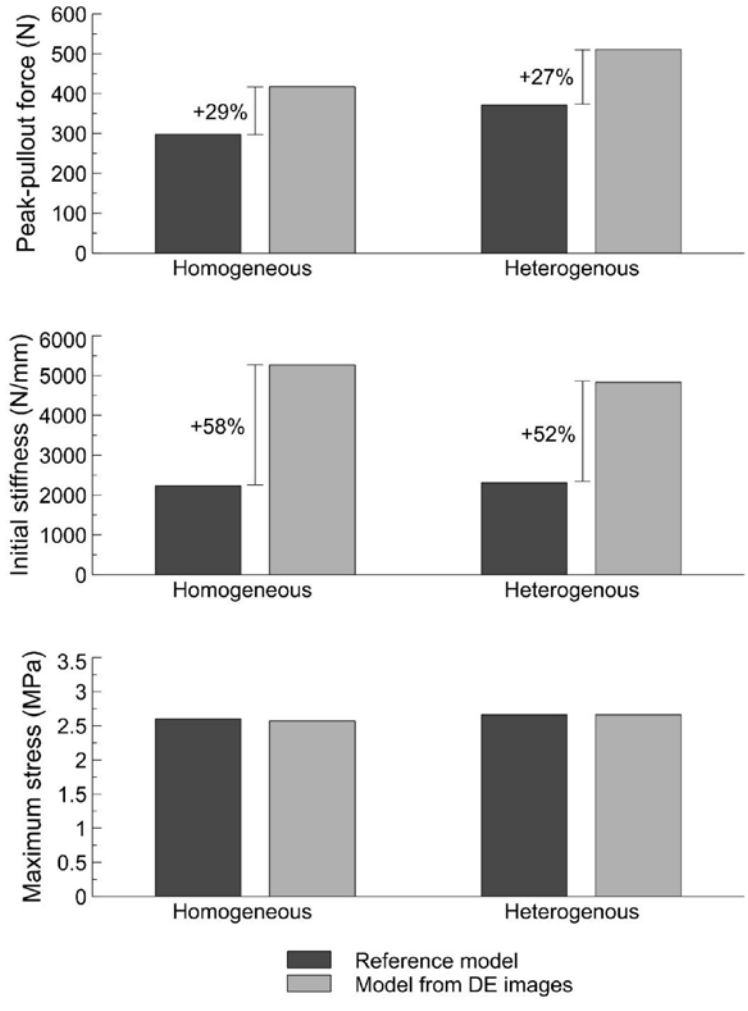

Figure 7. Simulation results of pedicle screw pull-out for the homogeneous and heterogeneous models with properties derived from DE images (light grey) and reference models (dark grey). The increase in peak pull-out forces and initial stiffnesses are reported. There was no difference for the maximum stress values.

along the entire length of the screw (Figure 5). The maximum stress was quite similar between all four models and ranged between 2.57 MPa and 2.66 MPa.

However, the force-displacement curves and initial stiffness were quite different between the four models (Figures 6 and 7). The initial stiffnesses for the models based on DE images were 5262 N/mm and 4830 N/mm for the homogeneous and heterogenous representations of the trabecular bone, respectively, while for the reference models it was 2232 N/mm and 2314 N/mm. Therefore, the stiffness of the models based on DE images was 58% and 52% higher than the homogeneous and heterogeneous reference models, respectively. The peak pull-out forces for the models based on DE images reached 418 N and 511 N for the homogeneous and heterogeneous models, respectively, while for the reference models, they were 28% lower (298 N and 371 N) (Figure 7).

The models based on DE images reached a peak pull-out force at a smaller simulated screw displacement than the reference models (0.1 mm vs. 0.15 mm, respectively) for the homogeneous models. The same tendency was seen for the heterogeneous models (0.14 mm vs. 0.2 mm).

Discussion

The novel DE imaging technology allowed to characterize the subject-specific mechanical properties, which had a clear impact on the simulation of screw pull-out vs. using published reference properties as done in most reported studies[16,25,48]. These differences are mostly seen in the

peak pull-out force during pull-out simulation and the initial stiffness of the bone-screw interface. This can be explained by the fact that the vBMD values of the DE images were slightly higher than those of the reference models (Tables 1 and 2), especially in the pedicle region where the vBMD is 3 times higher than in the posterior regions. Consequently, the posterior elements, the pedicles and the posterior regions of the vertebral body of the heterogeneous models had higher Young's modulus compared to the homogeneous models, which also contributed to higher pull-out force and stiffness. These differential properties cause the posterior subregions to provide better resistance at the first quarter of the pedicle screw length during simulated pull-out, as shown in [44], where it was found that the pedicle region contributes 80% of the bone-screw stiffness and 60% of the pull-out strength.

The observed relationship between bone density and resulting peak pull-out force is consistent with previous work reported, as well as the resulted screw pull-out forces which are found within reported value range[12], where the same type and dimension of pedicle screw were used. The initial stiffness of the current study is also comparable to or slightly higher than the values reported from experimental[49,50] and numerical[16] pedicle screw pull-out tests, adding confidence to the model presented in this study.

A strength of the DE imaging system used in this study is to provide calibrated HA radiographs, which allows a more precise quantification of the local mechanical properties of vertebral bone, to be incorporated in the vertebral FEMs, to the author's knowledge, a first study of its kind. Published studies have presented a similar work on estimating a heterogeneous representation of BMD distribution with single-image dual-energy X-ray absorptiometry (DXA)[51-53] and bi-planar radiography[54,55], but have not focused on quantifying mechanical properties for orthopedic instrumentation fixation.

The methodology presented in this study has shown the feasibility to evaluate bone quality from human vertebrae using the DE imaging system and could potentially be used on other bone structures, such as the femur, pelvis, humerus, or the mandible. Using more robust algorithms, regions of interest can be selected on different bone structures on the bone-calibrated radiographs, allowing an estimation of the mechanical properties. Furthermore, the contour-enhanced images provided by the system allow detailed definition of the bone structure of interest and thus improves the selection of the bone's geometry. This system could provide bone quality assessment with low-dose radiation (even lower than DXA) without compromising image resolution, an important factor when diagnosing bone disease, such as osteoporosis. Bone quality is a known parameter that affects screw fixation on spine instrumentation, and it is not usually considered in orthopedic surgical planning. The methodology shown in this study provides an insight into the capability of the DE imaging system to provide accurate representation of the bone mechanical properties and its use in numerical modelling, improving the decision-making for surgeons and decrease the risk of screw failure.

The limitations of this study include: 1) the need of manual identification of trabecular bone subregions to estimate the vBMD of vertebrae and therefore, the mechanical properties; 2) the absence of population data of DE radiographic images and therefore statistical analysis; 3) a segmentation limited for the moment to 8 subregions. An automatic algorithm would allow rapid calculation of volumetric bone density from bi-planar radiographs, especially since they can be matched via stereography methods. For the heterogeneous model, the manual definition of subregions must be done beforehand; this can be a tedious definition knowing that each subregion can vary from one patient to another. Having an automatic method to estimate the mechanical properties of a vertebra, and even more so, of a section or the entire spine, would allow faster acquisition of these properties for multiple radiographies. However, the estimation of vBMD is a first attempt to model the bone density in 3D based on a pair of radiographs. It is limited to being projectional and combining the superimposition of data. Further studies involving 3D reconstruction of the spine whilst embedding the projected biplanar HA-radiographs into the vertebrae geometry would help to refine and document the accuracy of the vBMD estimation.

Although limited to one case and one trajectory of a screw, this feasibility study confirmed the credibility of an approach based on DE radiographs to generate a vertebral FEM with subject-specific mechanical properties adapted to comprehensively study pedicle screw fixation and demonstrated the value of taking them into account to simulate instrumentation performance. Now that such demonstration is established, the approach can be applied to more cases and other screw dimensions and trajectories, which will eventually lead to a better understanding of inter-individual variations and to an appreciation of the importance of this tool for the design of better spinal instrumentation.

Conclusion

This study demonstrated the feasibility of vertebral FEM with subject-specific mechanical properties by exploiting the potential of low-dose bi-planar DE radiography. An increase on the biomechanical parameters measured during pull-out tests were seen on subject-specific models compared to reference models, indicating an important difference on including realistic mechanical properties on numerical models.

The ability to better describe the heterogeneity of bone density distribution in a vertebral FEM provides a relevant perspective to improve the quality of FEMs for orthopaedic surgery planning.

Acknowledgements

The authors would like to thank the Natural Sciences and Engineering Research Council of Canada (Industrial Research Chair with Medtronic of Canada) for sponsoring the scholarship of the Master student who conducted the study.

References

1. Inceoglu S, Burghardt A, Akbay A, Majumdar S, McLain RF. Trabecular Architecture of Lumbar Vertebral Pedicle. Spine 2005;30(13):1485-90.
2. Mabilleau G, Mieczkowska A, Libouban H, Simon Y, Audran M, Chappard D. Comparison between quantitative X-ray imaging, dual energy X-ray absorptiometry and microCT in the assessment of bone mineral density in disuse-induced bone loss. Journal of musculoskeletal & neuronal interactions 2015;15(1):42-52.
3. Banse X, Devogelaer JP, Munting E, Delloye C, Cornu O, Grynpas M. Inhomogeneity of human vertebral cancellous bone: systematic density and structure patterns inside the vertebral body. Bone 2001;28(5):563-71.
4. Briggs AM, Wark JD, Kantor S, Fazzalari NL, Greig AM, Bennell KL. Bone mineral density distribution in thoracic and lumbar vertebrae: An *ex vivo* study using dual energy X-ray absorptiometry. Bone 2006; 38(2):286-8.
5. Singer K, Edmondston S, Day R, Breidahl P, Price R. Prediction of thoracic and lumbar vertebral body compressive strength: correlations with bone mineral density and vertebral region. Bone 1995;17(2):167-74.
6. Christiansen BA, Kopperdahl DL, Kiel DP, Keaveny TM, Bouxsein ML. Mechanical contributions of the cortical and trabecular compartments contribute to differences in age-related changes in vertebral body strength in men and women assessed by QCT-based finite element analysis. J Bone Miner Res 2011;26(5):974-83.
7. Ryan PJ, Blake GM, Herd R, Parker J, Fogelman I. Distribution of bone mineral density in the lumbar spine in health and osteoporosis. Osteoporosis Int 1994; 4(2):67-71.
8. Augat P, Link T, Lang TF, Lin JC, Majumdar S, Genant HK. Anisotropy of the elastic modulus of trabecular bone specimens from different anatomical locations. Med Eng Phys 1998;20(2):124-31.
9. Fradet L, Vachon A, Levasseur A, Arnoux PJ, Petit Y. Prediction of bone anisotropic mechanical properties in osteoporotic human vertebral body from microstructural parameters. Comput Method Biomec 2013;16(sup1):326-7.
10. Keller TS, Hansson TH, Abram AC. Regional Variations in the Compressive Properties of Lumbar Vertebral Trabeculae - Effects of Disc Degeneration. Spine 1989; 14(9):1012-9.
11. Kopperdahl DL, Morgan EF, Keaveny TM. Quantitative computed tomography estimates of the mechanical properties of human vertebral trabecular bone. Journal of Orthopaedic Research 2002;20(4):801-5.
12. Liu S, Qi W, Zhang Y, Wu Z-X, Yan Y-B, Lei W. Effect of bone material properties on effective region in screw-bone model: an experimental and finite element study. Biomed Eng Online 2014;13(1):83.
13. Okuyama K, Abe E, Suzuki T, Tamura Y, Chiba M, Sato K. Influence of bone mineral density on pedicle screw fixation a study of pedicle screw fixation augmenting posterior lumbar interbody fusion in elderly patients. The Spine Journal 2001;1(6):402-7.
14. Bokov A, Bulkin A, Aleynik A, Kutlaeva M, Mlyavykh S. Pedicle Screws Loosening in Patients with Degenerative Diseases of the Lumbar Spine: Potential Risk Factors and Relative Contribution. Global Spine J 2019;9(1):55-61.
15. Galbusera F, Volkheimer D, Reitmaier S, Berger-Roscher N, Kienle A, Wilke H-J. Pedicle screw loosening: a clinically relevant complication? European Spine Journal 2015;24(5):1005-16.
16. Bianco R-J, Arnoux P-J, Wagnac E, Mac-Thiong J-M, Aubin C-É. Minimizing Pedicle Screw Pullout Risks. Clin Spine Surg 2017;30(3):E226-E32.
17. Hicks JM, Singla A, Shen FH, Arlet V. Complications of Pedicle Screw Fixation in Scoliosis Surgery. Spine 2010;35(11):E465-E70.
18. Hsu CC, Chao CK, Wang JL, Hou SM, Tsai YT, Lin J. Increase of pullout strength of spinal pedicle screws with conical core: Biomechanical tests and finite element analyses. Journal of Orthopaedic Research 2005;23(4):788-94.
19. Lai DM, Shih YT, Chen YH, Chien A, Wang JL. Effect of pedicle screw diameter on screw fixation efficacy in human osteoporotic thoracic vertebrae. J Biomech 2018;70:196-203.
20. Newcomb AGUS, Baek S, Kelly BP, Crawford NR. Effect of screw position on load transfer in lumbar pedicle screws: a non-idealized finite element analysis. Comput Method Biomec 2017;20(2):182-92.
21. Chao KH, Lai YS, Chen WC, Chang CM, McClean CJ, Fan CY, et al. Biomechanical analysis of different types of pedicle screw augmentation: a cadaveric and synthetic bone sample study of instrumented vertebral specimens. Medical Engineering & Physics 2013;35(10):1506-12.
22. Molinari L, Falcinelli C, Gizzi A, Martino AD. Biomechanical modeling of metal screw loadings on the human vertebra. Acta Mech Sinica 2021;37(2):307-20.
23. Faizan A, Kiapour A, Kiapour AM, Goel VK. Biomechanical Analysis of Various Footprints of Transforaminal Lumbar Interbody Fusion Devices. J Spinal Disord Techniques 2014;27(4):E118-E27.
24. Fradet L, Petit Y, Wagnac E, Aubin CE, Arnoux PJ. Spine Model for Safety and Surgery (SM2S): vers une caractérisation du comportement traumatique du rachis thoraco-lombaire. Morphologie 2013;97(318-319).
25. Abbeele MVd, Valiadis J-M, Lima LVPC, Khalifé P, Rouch P, Skalli W. Contribution to FE modeling for intraoperative pedicle screw strength prediction. Comput Method Biomec. 2017;21(1):1-9.
26. Poelert S, Valstar E, Weinans H, Zadpoor AA. Patient-specific finite element modeling of bones. Proc Institution Mech Eng Part H J Eng Medicine 2012;227(4):464-78.
27. Liebschner MAK, Kopperdahl DL, Rosenberg WS, Keaveny TM. Finite Element Modeling of the Human Thoracolumbar Spine. Spine 2003;28(6):559-65.
28. Guo L-X, Li W-J. Finite element modeling and static/

dynamic validation of thoracolumbar-pelvic segment. Comput Method Biomec. 2019;23(2):1-12.
29. Adam CJ, Askin GN. Lateral bone density variations in the scoliotic spine. Bone. 2009;45(4):799-807.
30. Chen Y, Dall'Ara E, Sales E, Manda K, Wallace R, Pankaj P, et al. Micro-CT based finite element models of cancellous bone predict accurately displacement once the boundary condition is well replicated: A validation study. J Mech Behav Biomed 2017;65:644-51.
31. Chevalier Y, Matsuura M, Krüger S, Fleege C, Rickert M, Rauschmann M, et al. Micro-CT and micro-FE analysis of pedicle screw fixation under different loading conditions. Journal of Biomechanics. 2018;70:204-11.
32. Presciutti SM, Karukanda T, Lee M. Management decisions for adolescent idiopathic scoliosis significantly affect patient radiation exposure. The Spine Journal 2014;14(9):1984-90.
33. Glocker B, Feulner J, Criminisi A, Haynor DR, Konukoglu E. Medical Image Computing and Computer-Assisted Intervention – MICCAI 2012, 15th International Conference, Nice, France, October 1-5, 2012, Proceedings, Part III. Lect Notes Comput Sc 2012:590-8.
34. Glocker B, Zikic D, Konukoglu E, Haynor DR, Criminisi A. Medical Image Computing and Computer-Assisted Intervention – MICCAI 2013, 16th International Conference, Nagoya, Japan, September 22-26, 2013, Proceedings, Part II. Lect Notes Comput Sc 2013: 262-70.
35. Wagnac E, Michardière D, Garo A, Arnoux P-J, Mac-Thiong J-M, Aubin C-E. Biomechanical analysis of pedicle screw placement: a feasibility study. Stud Health Technol 2010;158:167-71.
36. Keller TS. Predicting the compressive mechanical behavior of bone. Journal of Biomechanics 1994; 27(9):1159-68.
37. Zhao FD, Pollintine P, Hole BD, Adams MA, Dolan P. Vertebral fractures usually affect the cranial endplate because it is thinner and supported by less-dense trabecular bone. Bone 2009;44(2):372-9.
38. Wagnac E, Arnoux P-J, Garo A, Aubin C-E. Finite element analysis of the influence of loading rate on a model of the full lumbar spine under dynamic loading conditions. Med Biol Eng Comput 2012;50(9):903-15.
39. Carter DR, Bouxsein ML, Marcus R. New approaches for interpreting projected bone densitometry data. J Bone Miner Res 1992;7(2):137-45.
40. Garo A, Arnoux PJ, Aubin CE. Estimation of bone material properties using an inverse finite element method. Comput Method Biomec 2009;12(sup1):121-2.
41. Garo A, Arnoux PJ, Wagnac E, Aubin CE. Calibration of the mechanical properties in a finite element model of a lumbar vertebra under dynamic compression up to failure. Med Biol Eng Comput 2011;49(12):1371-9.
42. El-Rich M, Arnoux P-J, Wagnac E, Brunet C, Aubin C-E. Finite element investigation of the loading rate effect on the spinal load-sharing changes under impact conditions. Journal of Biomechanics 2009;42(9):1252-62.
43. El-Rich M, Wagnac E, Arnoux PJ, Aubin CE. Detailed modelling of the lumbar spine for trauma applications: preliminary results. Comput Method Biomec 2008; 11(sup001):93-4.
44. Hirano T, Hasegawa K, Takahashi HE, Uchiyama S, Hara T, Washio T, et al. Structural Characteristics of the Pedicle and Its Role in Screw Stability. Spine (Phila Pa 1976). 1997;22(21):2504-10.
45. Silva MJ, Wang C, Keaveny TM, Hayes WC. Direct and computed tomography thickness measurements of the human, lumbar vertebral shell and endplate. Bone 1994;15(4):409-14.
46. Bianco R-J, Arnoux P-J, Mac-Thiong J-M, Aubin C-E. Thoracic pedicle screw fixation under axial and perpendicular loadings: A comprehensive numerical analysis. Clin Biomech 2019;68:190-6.
47. Bianco RJ, Arnoux PJ, Mac-Thiong JM, Wagnac E, Aubin CE. Biomechanical analysis of pedicle screw pullout strength. Comput Method Biomec 2013; 16(sup1):246-8.
48. Xu M, Yang J, Lieberman IH, Haddas R. Finite element method-based study of pedicle screw–bone connection in pullout test and physiological spinal loads. Med Eng Phys 2019;67:11-21.
49. Inceoglu S, McLain RF, Cayli S, Kilincer C, Ferrara L. Stress relaxation of bone significantly affects the pull-out behavior of pedicle screws. Journal of Orthopaedic Research 2004;22(6):1243-7.
50. Abshire BB, McLain RF, Valdevit A, Kambic HE. Characteristics of pullout failure in conical and cylindrical pedicle screws after full insertion and back-out. The Spine Journal 2001;1(6):408-14.
51. Whitmarsh T, Humbert L, Craene MD, Barquero LMDR, Frangi AF. Reconstructing the 3D Shape and Bone Mineral Density Distribution of the Proximal Femur from Dual-Energy X-Ray Absorptiometry. Ieee T Med Imaging 2011;30(12):2101-14.
52. Humbert L, Martelli Y, Fonollà R, Steghöfer M, Gregorio SD, Malouf J, et al. 3D-DXA: Assessing the Femoral Shape, the Trabecular Macrostructure and the Cortex in 3D from DXA images. Ieee T Med Imaging. 2017;36(1):27-39.
53. Väänänen SP, Grassi L, Flivik G, Jurvelin JS, Isaksson H. Generation of 3D shape, density, cortical thickness and finite element mesh of proximal femur from a DXA image. Med Image Anal 2015;24(1):125-34.
54. Choisne J, Valiadis J-M, Travert C, Kolta S, Roux C, Skalli W. Vertebral Strength Prediction from Bi-Planar Dual Energy X-ray Absorptiometry under Anterior Compressive Force using a Finite Element Model: an *in vitro* study. J Mech Behav Biomed 2018;87:190-6.
55. Humbert L, deGuise JA, Aubert B, Godbout B, Skalli W. 3D reconstruction of the spine from biplanar X-rays using parametric models based on transversal and longitudinal inferences. Med Eng Phys 2009;31(6):681-7.
56. Kopperdahl DL, Keaveny TM. Yield strain behavior of trabecular bone. Journal of Biomechanics 1998; 31(7):601-8.